# scientific reports

OPEN

# Mapping decadal land cover dynamics in Sicily's coastal regions

Pietro Scala[1✉], Alexandra Toimil[2], Moisés Álvarez-Cuesta[2], Giorgio Manno[1] & Giuseppe Ciraolo[1]

Coastal zones are dynamic interfaces shaped by the interplay of Land Cover (LC) and Land Use (LU), influenced by both natural processes and anthropogenic activities. Grasping the historical shifts in land is essential for safeguarding coastal benefits such as defense mechanisms, biodiversity conservation, and recreational spaces, alongside enhancing their management. LC and LU products offer a valuable option for monitoring urban development, vegetation coverage, and dry-beach areas. Herein, we present the first study of the spatiotemporal evolution of LC specifically tailored for coastal zones, using the coast of Sicily as an illustration. We used classified satellite imagery from Landsat and Sentinel missions as input for a semantic segmentation model based on deep neural networks. We trained the model with an extensive dataset of coastal images. Our classification and analysis of coastal LC dynamics from 1988 to 2022 provide insights at a high spatiotemporal resolution. We identified key factors driving urban transformation, underscoring the impact of urban expansion on vegetated areas, and explored its correlation with economic and demographic growth. This study includes a multiscale analysis of coastal changes, encompassing long-term trends and seasonal fluctuations across Sicilian beaches. Our findings can contribute to preserve coastal areas by informing policymaking aimed at sustainable management.

Knowledge of Land Use (LU) and Land Cover (LC) changes is key information for effective management of agricultural production, natural resource use, and understanding of various environmental drivers such as local and global temperature regimes, precipitation, and shifts in biodiversity and ecosystem health[1,2]. These changes in LU are driven by many factors, including climatic variations on land[3,4] due to changes in rainfall patterns and vegetation, and rising temperatures. Additionally, human activities[5,6] can significantly affect LU through urbanization, deforestation, intensive agriculture, and infrastructure construction. Such practices can lead to a rapid transformation of the environment, thereby influencing LU trends. In coastal zones, these changes occur more rapidly due to the dynamic nature of these areas, which undergo changes at different temporal scales[7–9]. Coastal landscapes and shorelines are modified by erosion and sedimentation caused by waves and water levels and by anthropogenic interventions that have been deployed to protect communities from erosion and flood risks[10,11] and provide them with recreational services.

Historically, humans have settled along the coast where they have developed ports and commercial centers. Industrialization catalyzed the expansion and transformation of coastal cities, fostering infrastructure growth. Over the past six decades, there has been a significant shift of the population and economic activities towards the coast[12,13], which in turn has increased environmental degradation through deforestation, pollution, and habitat destruction. Degradation of dune vegetation can increase beach erosion, amplify coastal flooding and pose risks to both the tourism sector and the safety of coastal population[14,15]. Likewise, human-induced loss of coastal habitats can negatively affect both marine and terrestrial biodiversity[16,17]. The historical evolution of LU and LC reflects many of these dynamics and analyzing them can help understand the origin of changes, the pace at which they have occurred, and even what might happen in a few years[18–20]. This information can help improve resource and land planning[21,22], especially in coastal areas, with all indications pointing towards their continued growth in the future.

LC mapping has evolved considerably over the last 30 years. Initially this was done through visual analysis of aerial imagery[23,24], and then moved to automatic categorization of multispectral satellite imagery[25] using non-supervised[26,27] or fully supervised[28,29] approaches. In recent years, it has become increasingly common to use neural networks techniques[30] (especially CNN, convolutional neural networks) for of LULC maps detection[31–35]. Most of the LULC products available to date, which are not obtained from photo-interpreted datasets, have low spatial resolutions (1 km and 300 m for GLCC and ESA Land Cover - CCI respectively). In contrast, products obtained by state-of-the-art methods, such as Artificial Neural Networks, and with higher spatial resolution

[1]Department of Engineering (DI), University of Palermo, Viale delle Scienze, Bd. 8, Palermo 90128, Italy. [2]IHCantabria - Instituto de Hidráulica Ambiental de la Universidad de Cantabria, Isabel Torres 15, Santander 39011, Spain. ✉email: pietro.scala@unipa.it

---

(10 m) are still tested and validated through the use of visual photo-interpretation images (ESRI Land Cover[36,37]) without including datasets specific to coastal areas. Since the quality of the dataset is crucial to the classification process, complex environments such as the coast require a tailor-made solution. This is something that has not yet been fully developed to date. Although several LULC products have already been developed and used for the analysis of changes at different spatial scales, the real gap lies in coastal-specific LULC maps. The Coastal Zone[38] is the only LULC product specific to coastal environments but also obtained through visual interpretation and thus only available for two reporting years. While the ESRI 2020 Global Land Use Land Cover is obtained by employing artificial intelligence but being a global product and trained mainly with images of the hinterland, it is not specific and has gaps especially in coastal environments. Classifying coastal LC is a challenging task in remote sensing because of the complex and fragmented nature of coastal landscapes. Starting from the work of Liu et al.,[39], in which global-scale urbanization maps are provided for each year from 1985 to 2015, it can be seen that while from an urban perspective one map per year of coastal LULC is acceptable for coastal LULC, an annual map is not sufficient to capture both short- and long-term changes in, for example, beaches (the case of Coastal Zone product). On the opposite side[40] introduced a methodology for obtaining a high resolution (10 m) LULC map for Vietnam, using a CNN approach based on temporal rather than spatial features. Due to the aforementioned coastal dynamism and the complex nature-human interactions in coastal environments, it is of particular interest to obtain LC classifications specific to coastal environments. Especially at appropriate spatial and temporal scales and sampling intervals to capture their dynamism. A summary of the discussed LULC products and their acquisition methodologies, spatial and temporal scales (time sampling) is given in Table 1. All the LULC products reported in Table 1 are characterized by one map per reported years (e.g. ESA Land Cover – CCI, 1 image per year from 1992 to 2015).

A key novelty of our work is the use of a semantic segmentation model trained with an extensive dataset specific for coastal environments, the Coast Train[41]. We rely on state-of-the-art artificial intelligence techniques to recognize the characteristics of coastal environments and classify large coastal regions in short computational times and with high accuracy. Here, we showcased the methodology and its potential along the coast of Sicily (Italy). We developed an extensive hindcast of classified images for each month from 1988 to 2022, contributing significantly to the understanding of LC dynamics in this area over three decades. We acquired Landsat and Sentinel − 2b images and processed them using semantic segmentation techniques based on CNN. We correlated the LULC complex spatial model with scalar indicators such as socio-economic development. We conducted a historical analysis of the evolution of socioeconomic indicators of Sicilian coastal cities (population and income) in relation to coastal urbanization trends. We also investigated the evolution of the extent of Sicilian beaches, on an annual and seasonal basis, highlighting erosion and accretion over the three decades under study.

The main objective of this study is therefore to obtain coastal maps over time classified using a specifically trained model and to analyze the resulting coastal dynamics by exploring trends in variations of land cover classes and the main sources of conversion, providing information relevant for coastal management policies.

| Published products | Training dataset | Classification method | Time window | Map spatial scale | Spatial resolution | Overall accuracy |
|---|---|---|---|---|---|---|
| GLCC (Global Land Cover Characterization) | - | Unsupervised classification | 1992 to 1993 | Global | 1 km | 60 % |
| ESA Land Cover - CCI | - | Combination product of global surface reflectance from different satellite missions | 1992 to 2015 | Global | 300 m | 71 % |
| Witjes et al., 2022 | LUCAS and Corine Land Cover datasets | Spatiotemporal ensemble machine learning framework (Random Forest – Gradient-boosted trees – Artificial Neural Network) | 2000 to 2019 | Europe | 30 m | 83 % |
| Coastal Zones LC/LU | - | Visual interpretation | 2012 - 2018 | Europe (730,000 km2 of coastal landscape up to 10 km inland) | 10 m | 85 % |
| ESRI Global Land Use Land Cover | Dataset of more than 5 billion Sentinel-2 pixels, manually labelled | Deep Learning model based on U-Net | 2017 to 2022 | Global | 10 m | 75 % |
| Abdullah et al., 2019 | Dataset of pixels7areas identified through photointerpretation | eXtreme Gradient Boosting and Random Forest classifier | 1990 to 2017 | Coastal Region of Bangladesh | 30 m | 82 % |
| Feng et al., 2019 | Training and testing sample dataset derived from visual inspection | Multibranch convolutional neural network | 2018 | Yellow River Delta (China) | 10 m | 90 % |
| Liu et al., 2020 | ESA – CCI Land Cover product | Analysis of surface reflectance data from Landsat satellites in Google Earth Engine shell | 1985 to 2015 | Global | 30 m | 80 % |

**Table 1.** Collection and comparative analysis of LC data products across varied spatial scales.

## Study area

Sicily, the largest island in Italy and the Mediterranean, boasts a topography dominated by hills and mountains, with a coastline that serves as a major attraction. From the coastal perspective, Sicily, has a coastline stretching approximately 1600 km, characterized by diverse coastal settings varying in geology, shapes, marine climates, human influence, and more. Approximately 30% of this coast is rocky, transitioning between shallow carbonate platforms and elevated rocky cliffs. The remaining 70% primarily consists of sandy or pebbly shores, which are often long and subject to erosion, prompting demands for local government intervention. As already suggested in[42] in this research we will refer to the Sicilian coast into three significant segments: firstly, the Tyrrhenian segment from Boeo Cape to Peloro Cape (Thyrrenihan sea); secondly, the Ionian segment from Peloro Cape to Passero Cape (Ionian sea) and thirdly, the Central Mediterranean stretch from Passero Cape back to Boeo Cape (Mediterranean sea). We will refer hereinafter to these three macro-regions. A concise representation of Sicily and its geographical location is shown in Fig. 1. Considering this territorial complexity and transformation trough years, is surprising that there is still a lack of a complete picture regarding LC changes in coastal Sicilian areas, which are certainly characterized by areas with complex and heterogeneous coastal landscapes. The 2020 Regional Plan Against Coastal Erosion (PRCEC) is currently the only cognitive tool for coastal land in Sicily.

The communities of Sicily's coastal centers show considerable variation in size and demographic composition. Large coastal cities such as Palermo, Trapani and Catania have hosted dense populations due to their strategic location and sea-related economic opportunities. However, in recent years, there has been a considerable exodus from these cities to neighboring towns, probably due to declining quality of life in the main cities. In addition, Sicily has suffered protracted depopulation, mainly due to the migration of young people seeking work or educational opportunities elsewhere. Socioeconomically, Sicily's coastal centers present a diverse range of situations. Some benefit from prosperous economies related to tourism and maritime activities, particularly those with private marinas (e.g., Marina di Ragusa), while others face more significant economic challenges due to a dearth of job opportunities, especially in smaller communities. These conditions have contributed to a
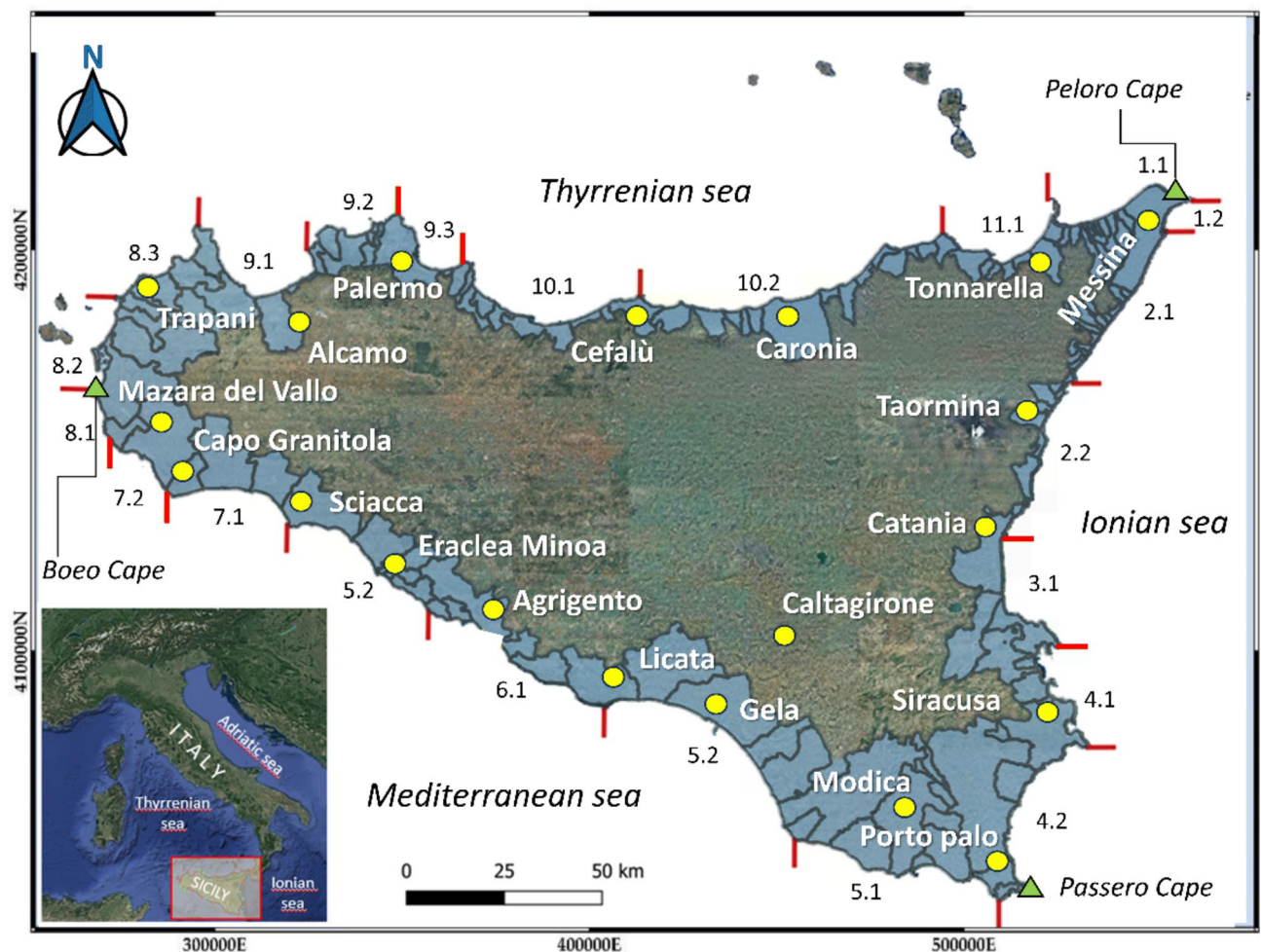


**Fig. 1**. Representation of Sicily, depicting Coastal Municipalities (CMs) in shaded blue areas, LICELs (LCs) segments in red, and highlighted locations (yellow points) referenced in the study (Reference System: WGS84-UTM33N-EPSG: 32633).

steady decline in Sicily's overall population in recent years, influenced mainly by residents of inland cities and towns.

## Results

### Validation of the model

To assess the CNN model's ability in segmenting various LC types and validate its performance, we implemented the methodology outlined in the "Methods" section across four distinct sites in Sicily. Each manually generated Ground Truth image covered an area of 10 km², totaling 40 km².

Figure 2 shows a graphical comparison between the reference satellite images (Capo Granitola, 2006, beach in panel A, the Catania airport area, 2013, in panel B, the Porto Palo coastal area, 2009, in panel C and the urban coastal center of Palermo, 2019, in panel D) and the ground truth by hand classified images (second line, respectively from E to H panel) with the images classified by the semantic segmentation model (third line, from I to L panel). As can be seen, the semantic segmentation provides the classification value predicted by the model at pixel scale. This comparison visually demonstrates the similarities and differences between the GT and model-generated LC classifications. The significant dissimilarities primarily arise from the nature of semantic segmentation, which delivers, as already reported, a pixel-level classification outcome, with each pixel classified based on the model's prediction. In this scenario, classes may exhibit greater fragmentation compared to GT images. However, semantic segmentation can yield more precise results in areas with elevated LC variability.

To validate the model results quantitatively as well as qualitatively, we estimated the degree of accuracy and coefficient $k$ (see "Methods"). The results are shown in Table 2.

The image validation results of four locations (Capo Granitola, Catania, Porto Palo, Palermo) are shown in Table 2. Each sub-table links the ground image to the model output, showing the number of correctly classified pixels for each LC class. The diagonals in bold indicate the correct detections, i.e. the pixels classified in the same way in the reference map and in the survey result (TPi). As can be observed, the detection of water pixels, for all images, is always above 98%. This is because the model used was extensively trained with coastal images. The results also show that no category (for any of the four images) has a Class Accuracy that is less than 50%. The lowest Class Accuracy values are for the Vegetation and Beach classes in the Capo Granitola map, for the Vegetation class in the Porto Palo map, and for the Vegetation and Bare Land classes for the Palermo map. The classes that show lower Class Accuracy than the others each time are the least frequent in each image. Conversely, the classes with a higher occurrence of pixels (e.g. Bare Land for Capo Granitola, Builtup for Catania and Palermo, and bare Land for Porto Palo) are always recognized by the model with an accuracy degree higher than 80%. For three out of four comparisons the class related to Beach always has a degree of accuracy greater than 60%. Only Capo Granitola shows a rate of 56%, but again the total number of pixels is significantly lower than those of the other classes. Overall, the comparison on Cape Grantiola shows an OA of 87.9%, Catania 88.2%, Porto Palo 82.3%, and Palermo 76.6%.
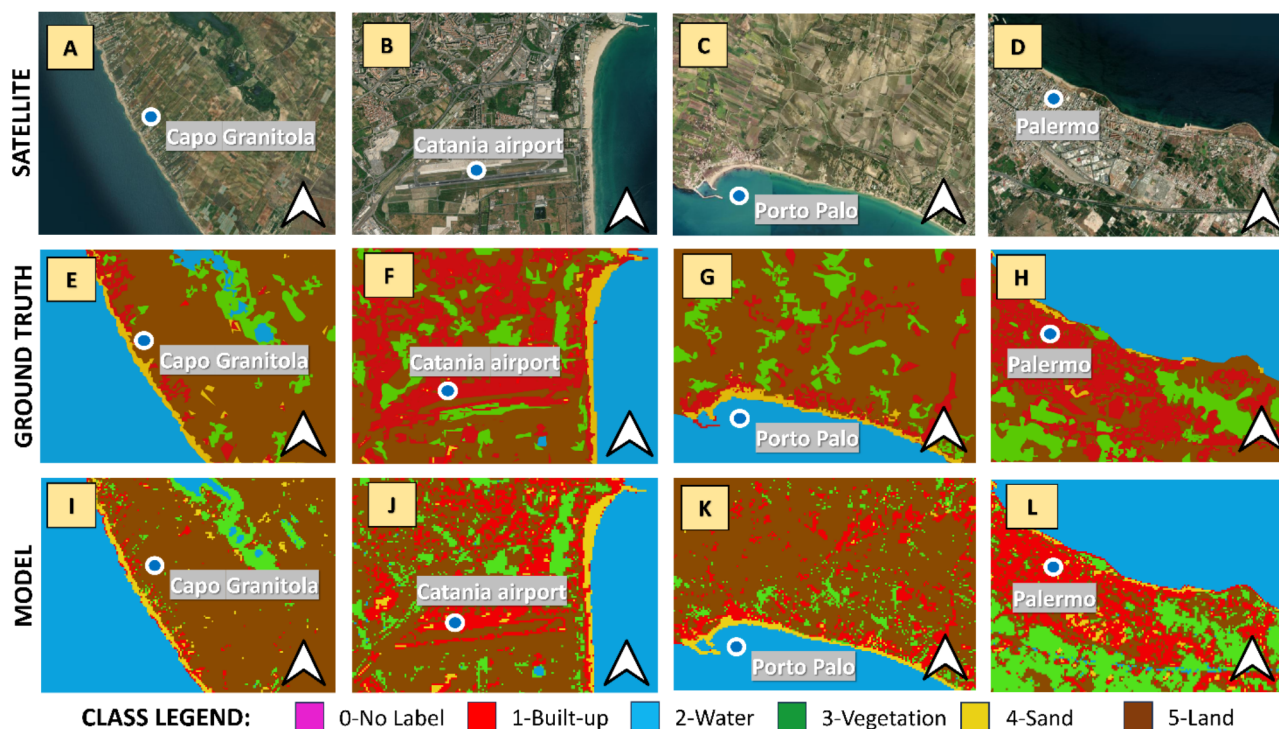


**Fig. 2.** Visual validation of the image segmentation algorithm at four coastal sites. Panels (**A–D**) (first row), (**E–H**) (second row) and (**I–L**) (third row) shows the reference satellite images, the ground-truth detection, and the model classification, respectively.

**CAPO GRANITOLA**
Model

| Class ID | 1 | 2 | 3 | 4 | 5 |
|---|---|---|---|---|---|
| 1 | **326** | 67 | 12 | 88 | 13 |
| 2 | 0 | **8057** | 54 | 0 | 8 |
| 3 | 26 | 279 | **688** | 9 | 217 |
| 4 | 103 | 68 | 6 | **394** | 128 |
| 5 | 595 | 18 | 795 | 183 | **11965** |
| *Class accuracy* | 64 % | 99 % | 56 % | 56 % | 88 % |

*Overall classification accuracy*: 87.9 %

*Kappa value*: 0.79

**CATANIA**
Model

| Class ID | 1 | 2 | 3 | 4 | 5 |
|---|---|---|---|---|---|
| 1 | **4820** | 18 | 118 | 29 | 481 |
| 2 | 4 | **3316** | 0 | 1 | 2 |
| 3 | 76 | 0 | **1018** | 0 | 333 |
| 4 | 35 | 54 | 0 | **405** | 1 |
| 5 | 303 | 1 | 546 | 16 | **5515** |
| *Class accuracy* | 88 % | 100 % | 71 % | 82 % | 86 % |

*Overall classification accuracy*: 88.2 %

*Kappa value*: 0.83

**PORTO PALO**
Model

| Class ID | 1 | 2 | 3 | 4 | 5 |
|---|---|---|---|---|---|
| 1 | **1448** | 10 | 84 | 113 | 643 |
| 2 | 3 | **3709** | 1 | 18 | 12 |
| 3 | 54 | 0 | **587** | 15 | 418 |
| 4 | 70 | 66 | 1 | **336** | 70 |
| 5 | 672 | 0 | 1266 | 28 | **10413** |
| *Class accuracy* | 63 % | 99 % | 55 % | 62 % | 84 % |

*Overall classification accuracy*: 82.3 %

*Kappa value*: 0.70

**PALERMO**
Model

| Class ID | 1 | 2 | 3 | 4 | 5 |
|---|---|---|---|---|---|
| 1 | **3076** | 51 | 43 | 55 | 1084 |
| 2 | 76 | **8339** | 11 | 2 | 54 |
| 3 | 668 | 3 | **1936** | 1 | 1063 |
| 4 | 32 | 7 | 10 | **320** | 80 |
| 5 | 1284 | 0 | 176 | 6 | **1759** |
| *Class accuracy* | 71 % | 98 % | 53% | 71 % | 55 % |

*Overall classification accuracy*: 76.6 %

*Kappa value*: 0.67

**Class ID** : 1 ) Builtup – 2 ) Water – 3 ) Vegetation – 4 ) Beach/Sand – 5 ) Bare land

**Table 2**. Quantitative validation at four coastal sites using confusion matrices where the pixels classified by the segmentation algorithm are confronted with the ground-truth detection.
Each diagonal (in bold) represents the correct detections. The classification accuracy, the overall accuracy and the kappa coefficients are displayed for each class.

Table 2 also shows the values of the k coefficient for each comparison, again obtaining Substantial Agreement (SA) or Almost Perfect Agreement (APA)[43] for each image analyzed. Specifically 0.79 (SA), 0.83 (APA), 0.7 (SA) and 0.67 (SA) for Capo Granitola, Catania, Porto Palo and Palermo, respectively.

Further validation, of a qualitative nature, of the classified images obtained is shown in the Supplementary Information (Fig. S1).

### Built-up area evolution

Figure 3 shows the time series of built-up areas for the localities of Salemi, Mazara del Vallo, Modica, Tre Fontane/Triscina, Marsala-Lido Signorino and Caltagirone, with a classified image (second column) showing the trend of the built environment in the years from 1988 (light blue) to 2022 (red) for the areas within the grey boxes in the satellite images of the first column.

In general, for all selected locations, the pixels (green to red) of new urbanization (post-1988) represent the majority of built-up pixels. The urbanization rates in relative terms were 380, 88, 435, 63, 142 and 485% of increase respect to 1988 builtup areas from Salemi to Caltagirone, respectively. For all of the locations analyzed, therefore, urban expansion occurred mainly in suburban areas, particularly for Salemi, Modica and Caltagirone. For Salemi it is possible to note one of the largest and "necessary" urban expansion that occurred in the years after 1968 (and thus included in the scale of visualization of this work) following the "Belice Earthquake" of magnitude 6.4 that affected the area in 1968. Similarly, for Caltagirone where we note the 485% building expansion (compared to 1988) that led to the construction of the new town and the growth of services and commercial activities and Modica with 435% due to the expansion of the city into the suburbs (also as a result of increased tourism).

### Spatial distribution of land cover changes

Figure 4 shows the spatio-temporal variation of the Vegetation class (subplot A), Bare Land (subplot B) and Built-up land (subplot C and D) from 1988 to 2022. For each class type, we provide the LC gains, losses and stable areas and the evolution of the builtup area, which has increased by 47.3% from 1988 to 2022. This graphical representation offers a comprehensive look into the evolving nature of Sicily's terrains over a span of 35 years. The northeast part of the Sicilian coastal area is characterized by a very dense presence of vegetation (top right area of panel A), which has remained largely stable over the years (except for losses near urban areas). In contrast, the southern area shows an almost complete absence of vegetation. This can be attributed to the fact that this latter part of Sicily is densely populated with greenhouses. The western region, on the other hand, has experienced the most significant loss of vegetation, 77% of the total vegetation loss on the entire island. A
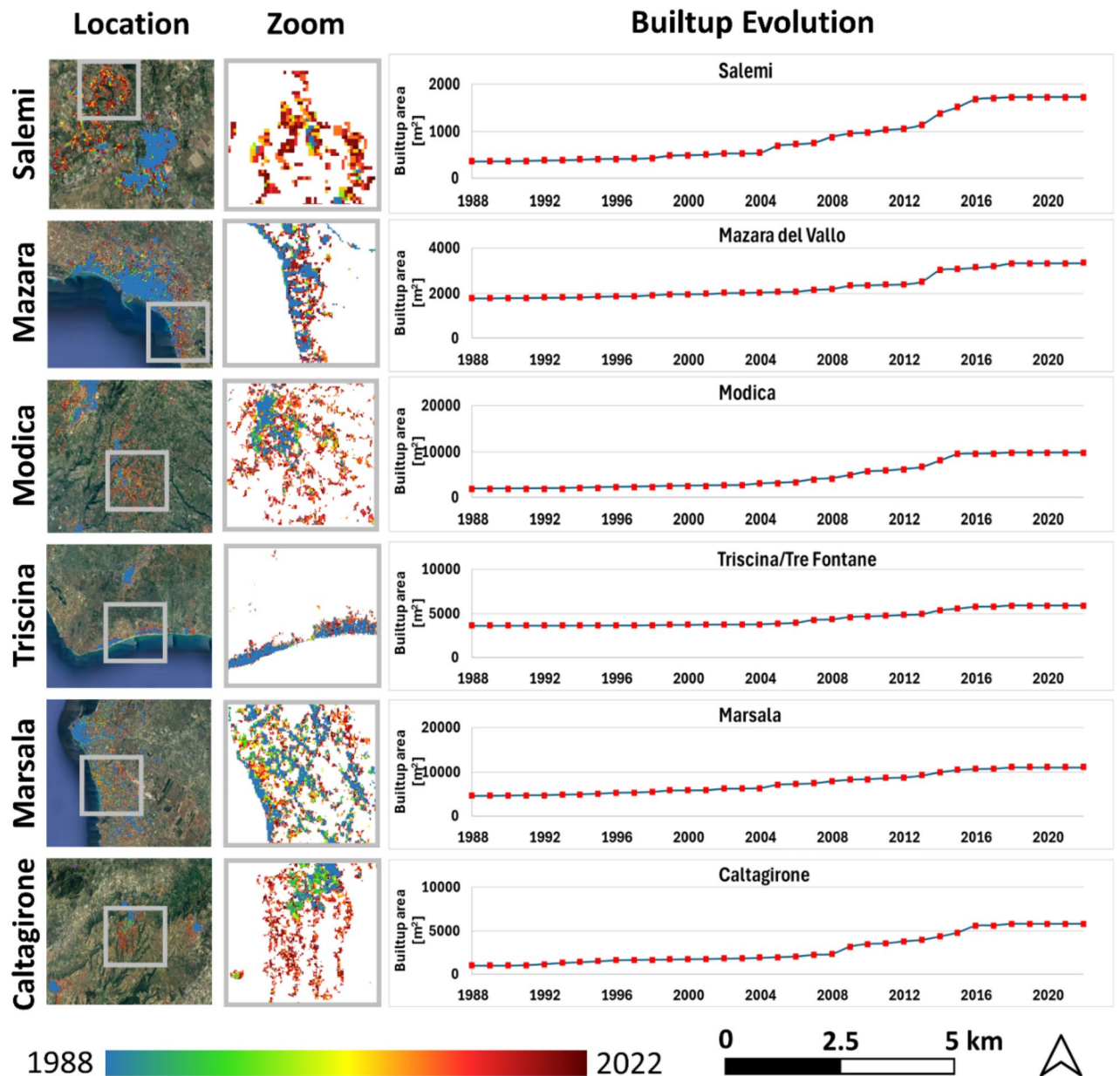
**Fig. 3**. Built up land expansion over the 1988–2022 period at six different cities: Salemi, Mazara del Vallo, Modica, Tre Fontane/Triscina, Marsala and Caltagirone. The second column shows the zooms (grey boxes in first column) temporal evolution of the builtup area overlaid with satellite images while the time series of built-up areas for all the localities is reported on the third column.

behavior almost opposite to that of vegetation is displayed by the bare land map (panel B). In this instance, where vegetation increases, there is a corresponding loss in bare land (50% of the entire bare land loss). Conversely, where vegetation decreases not due to human causes, a form of desertification might occur, leaving the ground as bare soil.

More details on trends over the years for LC classes are in the Supplementary Information (Figure S2).

### Changes in conversion sources for urban areas

Figure 5 shows the impacts of urban growth on major LCs (Vegetation and Bare Land) for each coastal municipality in absolute and relative terms over the period 1988–2022. The spatial representation of Sicily in the same figure shows the primary source of conversion of built-up area expansion in each CM. As can be observed, all the coastal municipalities in the north/northeastern part of Sicily have experienced expansion at the expense of the vegetation class. The opposite holds true for bare land. As described in Fig. 4, the spatial subdivision of the two classes is apparent. During the period considered, the trend is always increasing for both vegetation
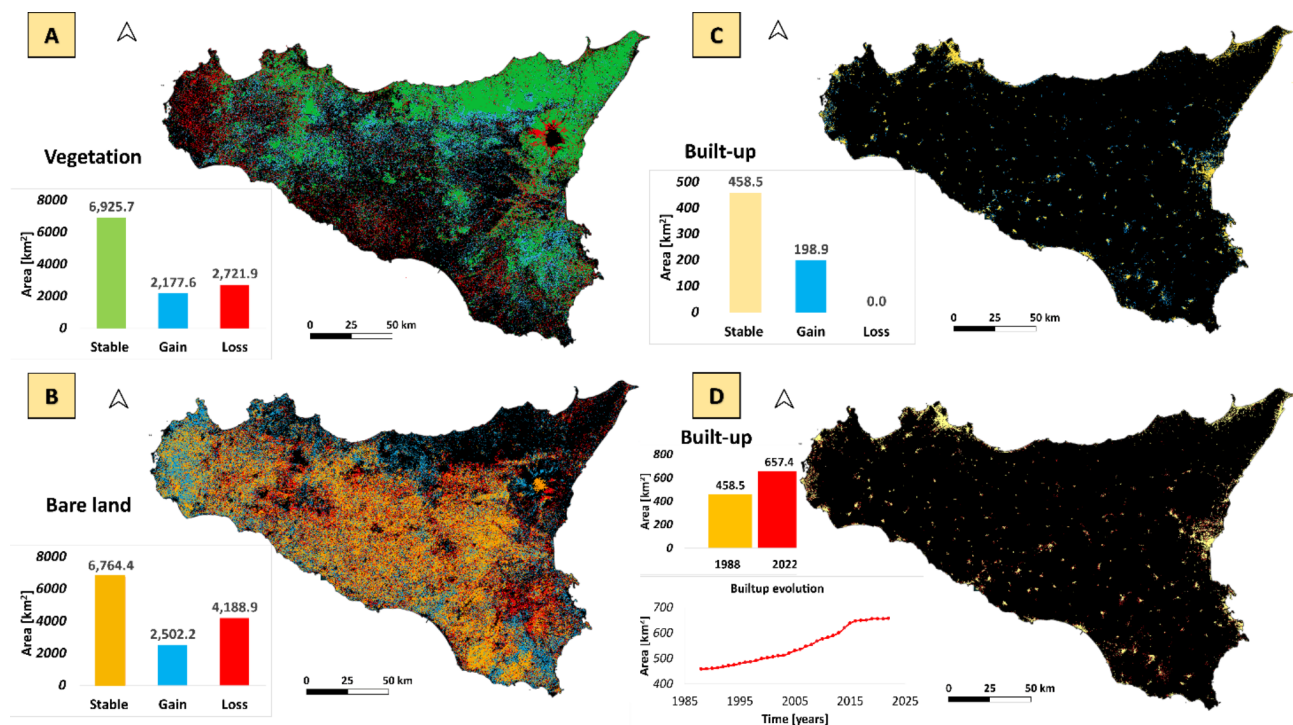
**Fig. 4**. Spatial distribution of stability, gains and losses in vegetated (subplot (**A**)), bare-land (subplot (**B**)) and built-up area (subplots (**C**) and (**D**)) in Sicily between 1988 and 2022. Each subplot illustrates the variations in LC types, accompanied by a summary bar plot indicating gain, loss, and stable area values (subplot (**A–C**)). The time trend and relative bar plot of the built up on regional scale is shown in subplot (**D**).
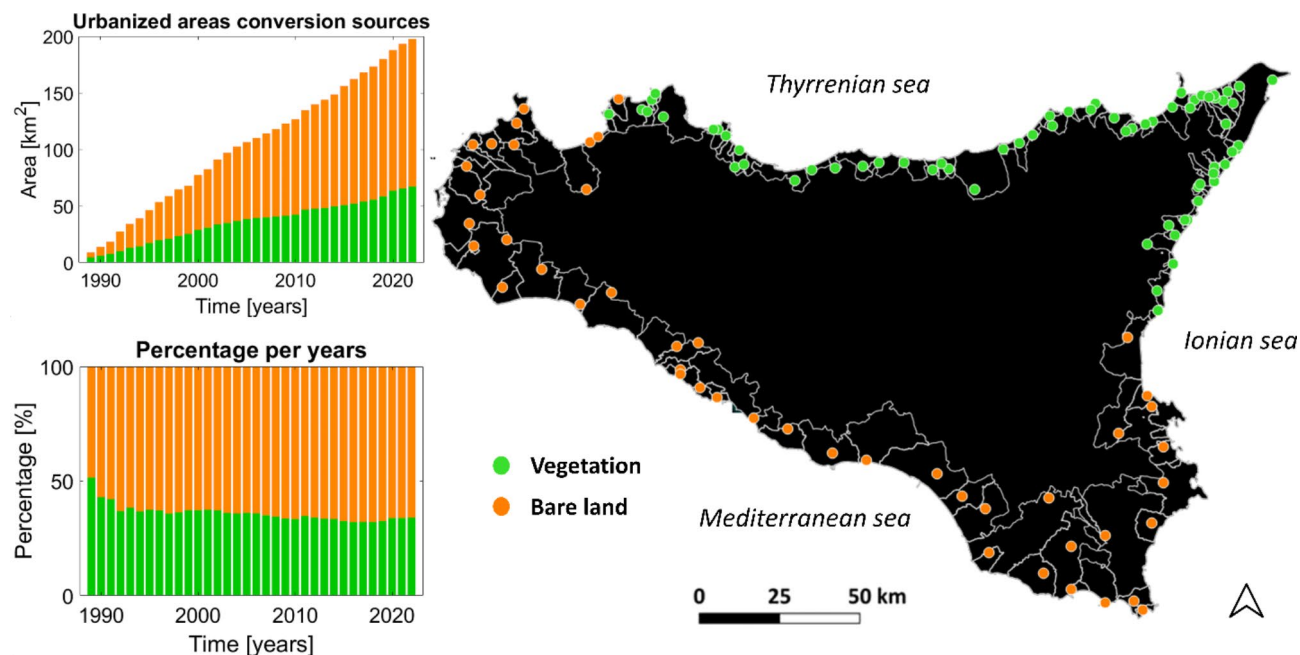


**Fig. 5**. Impacts of urban growth on the main LUs (vegetation and bare land) for each coastal municipality in absolute (**a**) and relative terms (**b**) over the 1988–2022 period. In panel (**c**) the primary conversion source of built-up area expansion is highlighted in each coastal municipality.

and bare land. In particular, there was an increase of about 20 times the 1988 urbanized area conversion value for the bare land class and about 7 times for the vegetation class. In the recent years (2017–2022), a growth trend has been observed in the built-up class, which is mirrored by a similar trend in the vegetation class. This suggests that the limited urbanization that occurred during this period had a more pronounced impact on the bare land class. In the early years, vegetation and soil values are similar or close in percentage terms, suggesting that there is a balance between the two. However, over time, a significant change is noted. The fact that the percentage of vegetation decreases relative to bare land indicates that building expansion has had a greater impact on vegetation than on bare land. In fact, while the vegetation class has a decrease from 54 to 34%, the bare land class shows the mirror-like trend. This means that as urbanization has progressed, green areas, such as forests or cultivated areas, have been converted into built-up areas. This has resulted in a significant reduction in vegetation. The rapid decrease in vegetation until 1992 (from 54 to 39%) suggests that there were very intense land transformations during that period, which led to a rapid loss of vegetation. After 1992, the decrease in the percentage of vegetation continued, but at a slower, almost constant rate. This could indicate that soil transformations have stabilized, with fewer vegetation conversions to unvegetated land, or that the remaining vegetation areas have been more effectively conserved.

### Changes in urban areas and correlation with socioeconomics

Figure 6 shows the correlation between these LU shifts and their relationships with various socio-economic indicators. The trend tests, all statistically consistent according to the Mann-Kendall test (p-value always less than 0.05), reveal distinct patterns. Coastal areas between the Mediterranean and Ionian stretches show a predominant population increase (first subplot to the left of the first row), while Tyrrhenian CMs generally experience depopulation, with some reversal west of Palermo (Gulf of Castellammare). In terms of income trends (second subplot from the left of the first row), negative patterns are observed in most Mediterranean municipalities, while the Tyrrhenian and Ionian CMs are more heterogeneous. The Mediterranean coastal area shows the highest urbanization trends, followed by the Ionian area, whereas the Tyrrhenian CMs, especially in the eastern part, exhibit fewer positive trends. In the second row of Fig. 6, contrasting trends are evident between built-up evolution and population. Sciacca experiences population growth of 3.9%, while other CMs show population decreases of 12.3% for Palermo, 25.5% for Caronia, 16.7% for Catania, 18.6% (a smaller decrease of 7.1% until 2017 and then a steep decrease) for Trapani and 5.3% for Gela. Caronia and Sciacca record the largest relative percentage increases in built-up areas (78% and 79.6%, respectively), which can be attributed to civil infrastructure development. Conversely, Palermo, Catania, Trapani, and Gela exhibit more moderate increases in built-up areas (8.4%, 22.1%, 43.5%, and 33.8%, respectively). Trapani, despite a decreasing population since 1988, shows a recent slowdown in population loss.
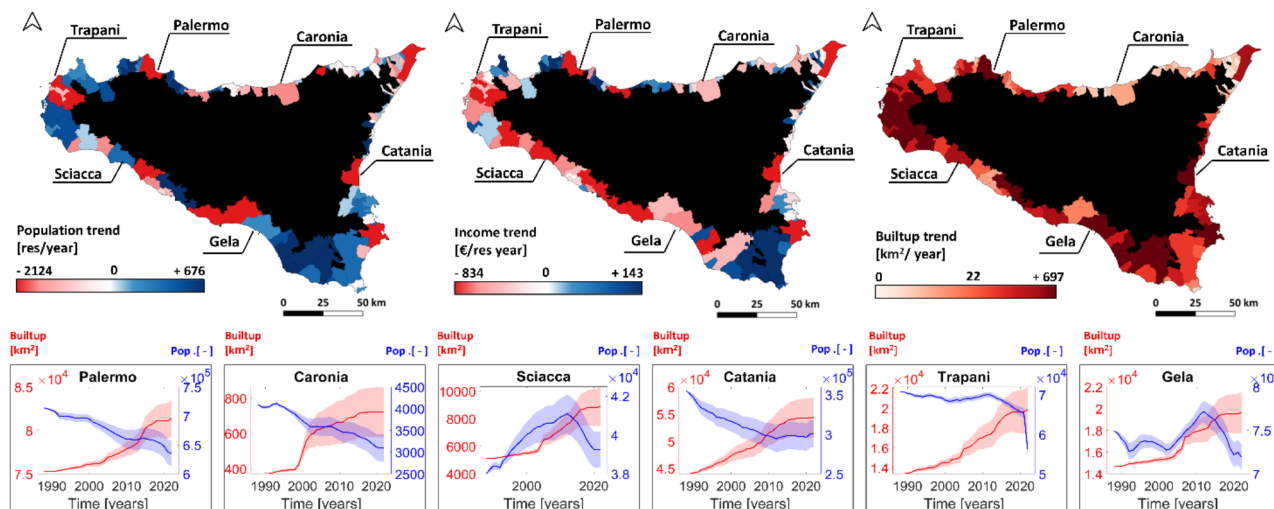


**Fig. 6.** Urbanization and LC dynamics in Sicilian coastal cities: correlating builtup area, population, and income trends from 1988–2022. In the figure's first column, for each CM, population, income, and built-up area trends are shown. The second row presents trends in built-up areas (red) and population (blue) for six CM, with respective variance bands for each timeseries. Axis annotations indicate specific category values.

Also in Fig. 6, it can be seen how, over time, the urbanization of the large Scillian cities (e.g. Catania or Palermo) has grown at a high rate and a decline in the city's population. In fact, incomes have also fallen in these areas, probably due to unrestrained building in the periphery that may not have contributed significantly to the growth of the local economy. It is necessary, however, to point out how the trend scales, which while also showing positive values, are predominantly unbalanced for both population and income. In fact, the color graded scales in the first row of Fig. 6, show a significant imbalance between negative and positive trends. We obtained negative maxima of -2124 res/year and −834 €/res year, while positive ones stop at +676 res/year and +143 €/res year for population and income, respectively. Finally, we found no clear correlations between population and urbanization. In fact, observation of decreasing population, increasing urbanization and variable, but often decreasing trends within LC areas reveals a complex picture of socioeconomic and environmental dynamics in Sicilian coastal communities.

For a greater understanding of the correlations between the built environment and the socioeconomic indicators analyzed, we created a map of the correlations between builtup, income and population (Figure S3 in the Supplementary Information).

### Changes in beach area dynamics

Figure 7 provides a visualization of beach erosion and accretion trends at the LICEL scale and the loss/gain conversion sources for beach areas. The figure also highlights year-on-year erosion, stability, or accretion trends (second row). Distinct behaviors of LICELs, such as LICEL 4.2, LICEL 5.2, LICEL 7.1 and LICEL 9.3, are showcased, underscoring the diverse coastal processes influencing each cell. As can be seen, the region showing strongly negative trends (ranging from 4 to 8.5% of beach eroded in 2022 compared to the initial beach values) is primarily in southern Sicily's coast (Strait of Sicily. In contrast, the beaches of the Tyrrhenian area of Sicily (North) have shown much lower decreasing trend values and even positive in some areas (LICEL 11.1 and LICEL 1.1 with percentage of increasing around 1–2% respect 1988 beach area values). Lastly, the Ionian area of Sicily (East) shows predominantly negative trends, especially in the south closer to the Strait of Sicily. Moving from Catania (in the middle) to the north of the Ionian stretch we reached mostly positive (accretion) trends (from 2 to 3.5% of beach increased in 2022 compared to the initial beach values). The observed erosion/accretion patterns align with wave energy variations in Sicily, consistent with findings reported by [44–47]. The comparison between these results and the values reported in PRCEC (2020) (see "Methods") are in Table S1 of the Supplementary Information.
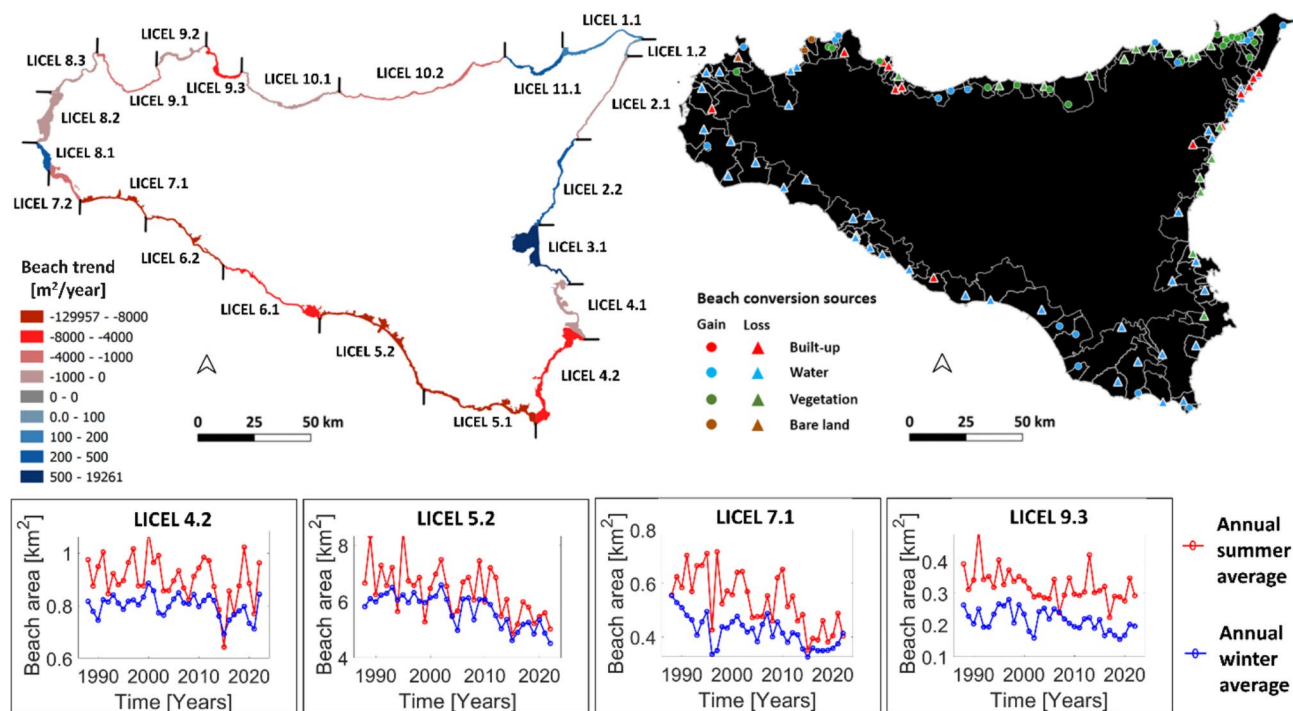


**Fig. 7.** Illustration of the LICELs temporal dynamics. The top left plot showcases the accretion and erosion trends expressed in km²/year. Dark blue indicates maximum positive trends, while dark red signifies maximum negative trends. In the top right plot, beach conversion sources for both loss and gain are represented for each CM, using triangles for loss conversion and dots for gain conversion. Colors represent conversion sources: red for Builtup, light blue for water, green for vegetation, and brown for bare land. The second row displays average annual trends in red for summer months (May to September) and in blue for winter months (November to March), explaining erosion, stability, or accretion trends for specific LICELs (in particular LICEL 4.2, LICEL 5.2, LICEL 7.2, and LICEL 9.3).

In the Mediterranean section (upper right panel), almost all of the beach conversion sources are of loss in favor of water. From the 109 cm studied, 36 belong to the Gain class while the remaining 76 to the Loss class. Thus, only 33% of Sicilian CMs show a predominance of gain beach conversion sources while 67% of loss conversion sources. In the western Tyrrhenian zone, there is greater heterogeneity in beach conversion sources with a few beaches showing gains on the vegetation (probably due to loss of dune vegetation) and bare land (beach advance due to sediment deposition) classes. The central-western zone of the Tyrrhenian section is the one most affected by beach loss conversion sources in favor of the builtup, while the eastern part shows losses and gains mainly on the vegetation class. The northern Ionian zone continues with the neighboring behavior of the Tyrrhenian zone while also showing losses due to builtup. In these areas the beach loss is very small (percentage) so the major conversions are caused by the fact that parts of these beaches are affected by the construction of bathing lidos. The southern zone of the Ionian section in turn fits to the neighboring Mediterranean zone showing a prevalence of loss conversion sources of water. Finally, in the second row of Fig. 7, LICEL 5.2, along with LICEL 9.3, displays the steepest erosion trend values, while 4.2, and especially 7.2, showcase less pronounced declining patterns. In relative terms of erosion or accretion, all the LICELs in the second row of Fig. 7 experienced (negative) erosion percentages. In particular 8.3%, 5.1%, 4.1% and 2.8% of beach erosion in 2022 relative to the initial beach values for LICEL 7.1, LICEL 4.2, LICEL 5.2 and LICEL 9.3 respectively. Furthermore, although the absolute values of loss for LICEL 8.2 and 2.1 were among the lowest of the sand losses in relative terms the beach loss was 15.8% and 5.6% respectively.

We computed, only 0.14 km$^2$ (0.2%) of beach in Sicily was converted to urbanized land between 1988 and 2022. This decrease can be attributable to the presence of many illegal properties along the coast, which represent 40–60% of the coastline[48,49]. Built in the 1970s without an approved plan, many of these summer residences have remained illegal despite amnesties and demolition orders. This persistent situation has caused lasting environmental impacts, including erosion, loss of biodiversity, and pollution of coastal and groundwater[50,51]. For further information, refer to the Figure S4 in Supplementary Information.

## Discussion

In our study, we conducted an extensive retrospective analysis of classified imagery of the entire Sicilian coastal region for each month from 1988 to 2022. This analysis used images from Landsat-5, Landsat-7, Landsat-8, Landsat-9 and Sentinel-2b. These images were processed with semantic segmentation techniques based on CNN. Our primary goal was to fill the gap in high-resolution LICEL data by employing an advanced artificial intelligence model trained with a large database specifically designed for coastal areas[41]. Furthermore, this research contributed to generating an extensive dataset that was previously nonexistent, enhancing the scope and specificity of coastal LC analysis.

The presented classification method resulted in coastal classifications with a high degree of accuracies (as described in the validation process) compared to the products available to date (seventh column of Table 1), which present overall accuracy in the range of 60[5,52], 71[53] and 75[54] percent for GLCC, ESA Land Cover - CCI and ESRI Global Land Use Land Cover, respectively. We also point out that products obtained purely for coastal areas (Coastal Zones LC/LU, Feng et al.[37]) show higher accuracy percentages, 85[55] and 90% respectively confirming the need for specific maps for these types of environments. The use of specific, appropriate and accurate datasets processed through machine learning algorithms, as in Witjes et al.[56], also achieves good overall accuracy values in the classifications (83%) confirming again how crucial the quality of the training data is. In our work we combined these concepts using a purely coastal dataset and obtained 35 years of monthly classified maps of maximum overall accuracies of 88%.

By obtaining this accurate classified data we were able to explore the socioeconomic evolution of Sicilian coastal municipalities in relation to coastal urbanization dynamics. The analysis represents a first step towards the understanding of land-use dynamics in this region over three decades, focusing on urban expansion, land-use changes, and changes in Sicilian beaches over the period under consideration. Our approach sheds light on the intricate relationship between socio-economic development and coastal land use changes and underscores the utility of cutting-edge AI techniques in enhancing our understanding of environmental dynamics in coastal areas.

The "Results" section, as well as validating the methodology adopted, delves into the LC dynamics in Sicily. The temporal evolution of built-up areas reveals urban sprawl in coastal municipalities, emphasizing variations in growth rates. Spatial distribution analysis highlights distinct patterns in Vegetation, Bare Land, and Builtup Areas, offering insights into environmental dynamics along the Sicilian coast. The sources of change in LC indicate direct influences of urban growth on vegetation conversion. An in-depth overview of erosion and accretion dynamics along Sicilian beaches, emphasizing LICELs is provided. Urbanization contributes modestly to beach loss, with illegal ownership being a significant factor, causing lasting environmental impacts. With the available data, we did not find a direct correlation between urban sprawl and socio-economic indicators. This fact highlights the complexity of linking LC changes with socio-economic dynamics such as income and population. The analysis of potential correlations of LC with met-oceanic data can also benefit future research.

Integrated management strategies are crucial to preserve the coast of Sicily and any other coast worldwide amid the complex interactions between natural and anthropogenic factors. Understanding LC dynamics can contribute to improving current and future land planning by informing decision-making processes aimed at promoting sustainable coastal development and resilience. This research sets a foundation for further studies in coastal LC dynamics and highlights the need for continued monitoring and analysis of coastal environments in the face of ongoing and future challenges, including climate change and need for adaptation, using specific coastal datasets and with appropriate sampling intervals for short-term and long-term analysis.

Our study has some limitations that may be potential areas for improvement. The first limitation is related to the training dataset. Despite Coast Train is specific for coastal regions its representativeness may not be

exhaustive in fully covering the variability of the Sicilian coast, since the selection of images may not include all possible variations in the island's coastal features. With that in mind, we manually selected images reflecting similar color characteristics, beach sizes, and urbanized contexts to those in Sicily. This careful selection provided the model with a diverse range of examples, ensuring a good level of generalization during the classification phase. In addition, we reviewed the results and made the required corrections. For example, greenhouses were misclassified by the model as built-up areas. The absence of these features in the training dataset meant the model struggled to classify them correctly. To address this issue, we created a mask to eliminate the false information caused by the greenhouses.

The second limitation is the statistical methods used, such as the Mann-Kendall test and correlation analysis, which may not account for the complex interactions between socioeconomic factors and changes in land cover, suggesting the need to consider more sophisticated nonlinear multivariate approaches in future studies.

The last limitation could be represented by the limited number of classes used in the semantic segmentation model, which includes 5 categories. Although this approach is suitable for regional scale analyses, it may not be sufficiently detailed for local studies that require higher precision on high-resolution images and thus a larger number of classes to represent. Improving the ability of the semantic segmentation model to distinguish a wider range of classes may therefore be useful to enable a more accurate interpretation of coastal landscape features in high spatial resolution contexts.

## Methods
This section describes the all the materials and methods used in the work.

### Methodology architecture
In order to analyze LC changes in Sicily from 1988 to 2022 we developed the methodology presented in Fig. 8. We employed a semantic segmentation model to process satellite images from Landsat and Sentinel datasets. This allowed us to create classified images of the entire Sicily for each month within the specified time frame. These images helped us identify different LC classes, including Water, Vegetation, Beaches, Bare Land, and Built-up areas. To ensure the accuracy of our results, we validated our model by comparing its classified images with ground truth images. Once we achieved a satisfactory level of accuracy, we conducted a comprehensive data analysis to understand the nature of the changes.

The research focused on the transition of LC to urban areas, quantifying growth rates, loss and stability in vegetation, bare land and built-up areas. The analyses we have conducted were devoted to the impacts of increasing urbanization, considering the complex relationship with urban expansion, population growth and income patterns, which are fundamental to interpreting social, economic, and environmental consequences. In addition, the analysis of LICELs in Sicily assessed trends in beach areas, highlighting the regions that are most susceptible to change and revealing whether they were accreting or receding.

### Satellite images used
The core of our methodology is based on the acquisition and processing of satellite imagery, covering the period from 1988 to 2022, to obtain a monthly, detailed view of Sicily's changing landscape. The imagery was sourced from various satellite platforms, including Landsat 5, 7, 8, and the more recent Landsat 9, as well as Sentinel 2. The satellite images were acquired with a spatial resolution of 30 m (Sentinel products with 10 m resolution but upscaled to 30 m resolution in order to work with a single resolution) using the Google Earth Engine (GEE) shell. We used a bilinear interpolation method for downsampling. This method was chosen to maintain a smooth transition between pixels and minimize information loss[57,58], visually examining the images to identify any artifacts or loss of significant detail.

We primarily focused on the RGB bands of satellite images to capture a vivid representation of the Earth's surface.

Central to our satellite image acquisition methodology was the stringent requirement of cloud cover, which we set at or below 20%. This criterion was essential to ensure that the images we used for our analysis were as clear and free from atmospheric distortions caused by cloud cover as possible. Our objective was to provide the subsequent semantic segmentation model (as detailed in the following section) with high-quality, clear input images. To achieve this, we meticulously selected images that met this specific criterion. Subsequently, each image underwent a cropping process, via QGIS raster tools, to obtain an identical extent of 512×512 pixels for each resulting image. In total, therefore, we obtained for each monthly image 280 images of 512×512 pixels resolution (so as to cover the entire extent of Sicily). Considering 12 images per year (one per month), over 35 years, the total number of images acquired was 117,600.

### Littoral cells, coastal municipalities, and socio-economic indicators
For the study of coastal dynamics and erosion/accretion movements, we divided the Sicilian coastline into 22 secondary-level shoreline segments (LICELs). Each segment, or sediment cell, has distinct sources of sediment, transportation routes, and deposition areas, making it an individual unit for management purposes[42].

In this paper, we defined "Coastal Area" as that portion of land that extends from one LICEL boundary to the other with landward extension delimited by areas with elevation less than or equal to 15 m. Coastal zones are usually considered to be the areas between 0 and 10 m[59]. In this case, we have extended the 10 m limit to 15 m. This choice is justified considering that Sicilian beaches are predominantly sandy and characterized by a low slope (1–3%), with an average width of about 60 m. The mask thus defined proved to effectively include all beaches, ensuring an accurate representation of the areas of interest. The 15-meter threshold made it possible to exclude headlands, focusing attention on beaches, which by their nature have greater dynamism. In addition, this extension also made it possible to include the urbanizations closest to the beaches, which are essential for
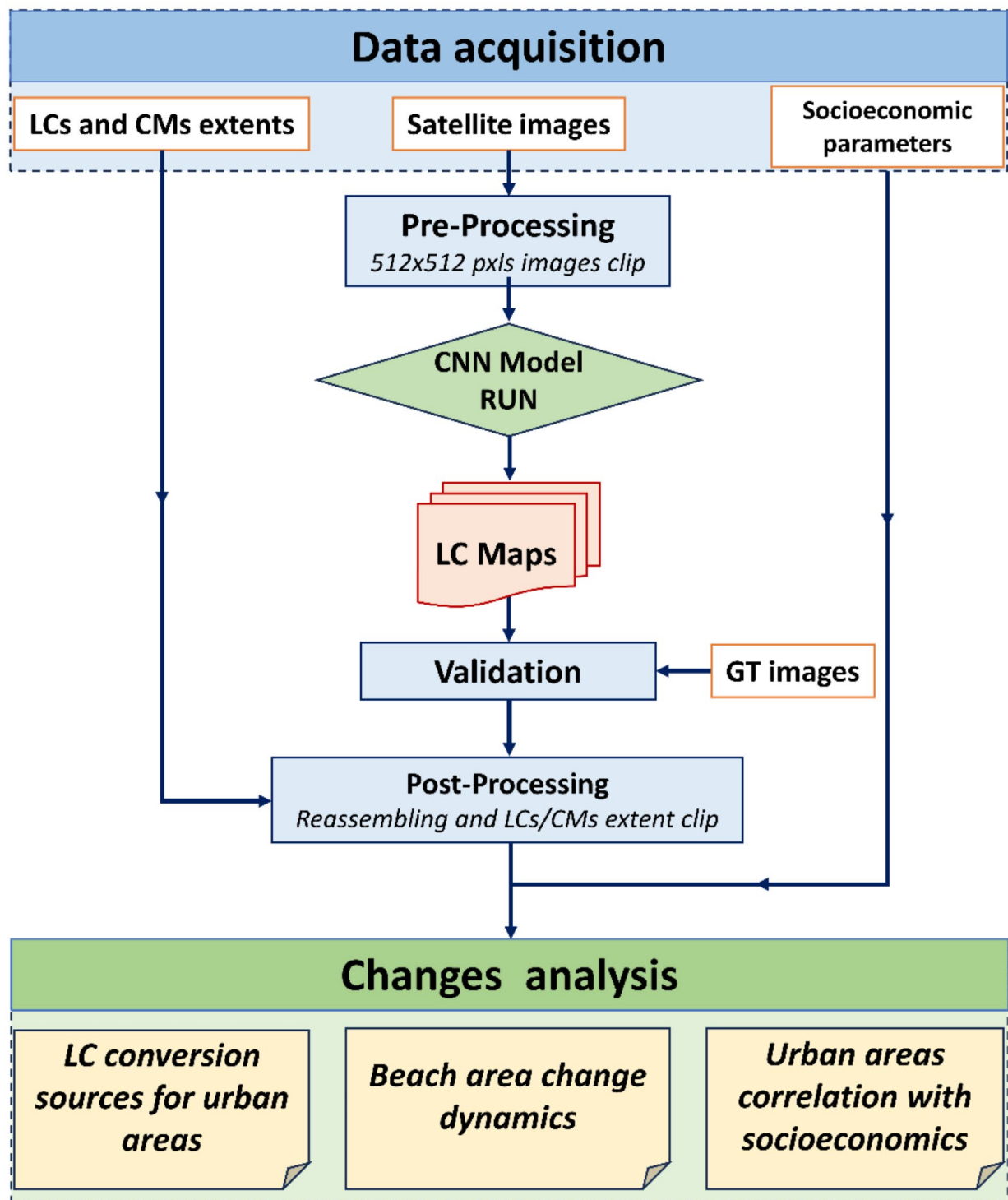
**Fig. 8**. Constructed methodology for analyzing changes in Land Cover.

a comprehensive analysis of the interaction between the coastal environment and human settlements that press directly on the beaches. We obtained the mask for the definition of these areas through the use of the Digital Elevation Model of the terrain (DEM) with $2 \times 2$ m resolution of the Sicilian Region.

We conducted the analysis of the correlation between changes in built-up area and changes in socio-economic indicators by defining the extent of each CM, 109 in total, through the shape file provided by the *Istituto Nazionale di Statistica* (ISTAT) regarding all the Italian municipal administrative boundaries. We chose as socio-economic indicators the population and income data provided by the ISTAT and the Ministry of Economy and Finance,

respectively. These data allowed us to examine demographic and economic trends over three decades and better understand the development dynamics at the scale of Sicilian CMs.

## Images segmentation process

In order to obtain the segmented images with respect to the following classes: (i) Builtup, (ii) Water, (iii) Vegetation, (iv) Beach and (v) Bare Land, we used a convolutional neural network (CNN)-based approach, which specifically adopts the U-Net architecture[60], for the critical detection task by semantic segmentation. This semantic segmentation model is a CNN model carefully trained using a rich image dataset al.ready labeled, known as the Coast Train dataset, consisting of numerous different season coastal imagery with 1.2 billion pixels labeled over 3.6 million hectares. The images, from sources such as NAIP, Sentinel-2, Landsat-8, USGS, and UAS, vary in resolution and cover coastlines other than the United States.

To ensure that the training dataset adequately represented the variability of the Sicilian coastline, we selected images that reflected similar color characteristics, beach sizes, and urbanized settings as Sicily. This selection was made by hand in order to provide the model with a variety of examples sufficiently diverse to ensure a good level of generalization during the classification phase. Although not all possible variants of the Sicilian coast were included, we focused on the most representative ones to effectively train the model. To avoid overfitting, the original dataset of 134 images was augmented using data augmentation techniques (e.g., cropping, rotation, brightness and contrast adjustment) with the Python Albumentations library[61].

The accuracy performance during the model training phase was around 85% while the Intersection over Union metrics around 75–80%. Therefore, in the present work we validated the segmentation capabilities of the model in consideration of the above metrics.

Once all the satellite images were processed through the semantic segmentation model, we reassembled them to obtain month by month a unique image of Sicily segmented through the classes mentioned above. In this way we obtained 420 classified images representing a huge dataset of satellite images with their respective LC masks, for a previously nonexistent observation period for the entire area of Sicily.

Regarding resampling and cropping effects, we point out that in the context of satellite image processing, each image can be represented as a three-dimensional matrix in which the three dimensions correspond to the red (R), green (G), and blue (B) color channels. Given a large initial image size, we can proceed to its cropping into sub-images of more manageable size while keeping the original resolution intact (e.g., $512 \times 512$ pixels for each sub-image). This subdivision process does not alter the original matrix: each pixel in the sub-images retains the same RGB color values it had in the global image. Therefore, if the classified sub-images are reassembled in their original positions, the source image is reconstructed without loss of information or distortion due to cropping, in order to obtain a coherent and continuous map of the entire island. This process ensures spatial continuity and consistency of the segmented classes, reconstructing an overall image that preserves the resolution and accuracy of pixel-level analysis. Semantic segmentation applied uniformly on each sub-image ensures that the classification is consistent over the entire study area. This pixel-wise approach ensures that the results are equivalent, regardless of whether the model operates on sub-images or the whole image. Therefore, the methodology adopted in our study preserves the integrity of the analysis even during the process of image cropping and reassembly.

## Segmentation validation

We used several indicators to determine the accuracy of the semantic segmentation model. Class accuracy, overall accuracy and Kappa coefficient were the main indicators used for this evaluation.

- Class accuracy[62,63], denoted as $AC_i$, measures the accuracy of the predictions of individual LC classes. The equation for class Accuracy is defined as (Eq. (1)):

$$AC_i = \frac{TP_i}{TP_i + FN_i},\tag{1}$$

Where $TP_i$ represents True Positives (correctly classified pixels) for class $I$ and $FN_i$ denotes False Negatives (pixels misclassified as not belonging to class $i$).

- Overall accuracy, often referred to as $OA$, provides a comprehensive assessment of model performance over all LC classes. It is calculated using the following equation (Eq. (2)):

$$OA = \sum \frac{AC_i}{n},\tag{2}$$

Where $\sum AC_i$ represents the sum of class accuracies for all LC classes and n indicates the total number of classes.

- The Kappa coefficient ($\kappa$)[43,64] evaluates the performance of the model considering the agreement between the predicted and reference classifications (Ground Truth, GT). It is calculated as (Eq. (3)):

$$k = \frac{(P_o - P_e)}{1 - P_e},\tag{3}$$

Where $P_o$ is the observed agreement while $P_e$ is the expected agreement by chance.

$P_o$ represents the fraction of cases in which the two image classifications (between GT and detection) agree. $P_o$ is calculated using the following equation (Eq. (4)):

$$P_o = \frac{Number\ of\ obesrvation\ in\ agreement}{Total\ EquationNumber\ of\ observation}. \tag{4}$$

$P_e$ represents the agreement that would be expected by chance. $P_e$ is calculated using the following equation (Eq. (5)):

$$P_e = \sum_{i=1}^{n} \frac{\sum row_i \sum column_i}{(\text{Total number of samples})^2}, \tag{5}$$

Where $n$ is the number of classes, $\sum row_i$ and $\sum column_i$ represents the sum of the values of the $i$-th row and $i$-th column respectively.

$k$ coefficient measures the agreement between predictions and Ground Truth, taking into account random matches; it is used to assess how much better the agreement is than would be expected by chance. In fact, note that the subscript i is not present in this case since the metric refers to the overall classification.

We conducted an accuracy analysis by comparing model predictions with reference images (GT) generated by manual classification. To provide additional qualitative perspective, further visual comparison was conducted with other existing LULC classification maps in the area of interest, including the based LUCAS dataset[56], Copernicus Coastal Zones maps and ESRI's Sentinel-2 10-meter LU and LC time series maps. These comparative assessments improve understanding of the effectiveness of the model in relation to existing methods and datasets and are presented in the Supplementary Information.

## Segmented images postprocessing

For the temporal analysis of each LC class areas, the classified images of the whole Sicily were cropped (for each month and year), using the CM and LC masks. Area values for each LC class were extracted. These area values represented the areas covered by each class in terms of the number of pixels (at a resolution of $30 \times 30$ m). In this way, the monthly area values (for each year) for each segmentation class were computed. Through this methodology, we conducted a temporal analysis of urban expansion in coastal municipalities and for other LU classes at both CMs and LICELs scales.

For the analysis of the Builtup class at the level of CMs, we considered an annual time scale, aggregating the monthly Builtup area data on an annual basis by averaging, since the monthly variations for this class were insignificant. On the other hand, for LICELs, the analysis was conducted at the monthly level, as we were interested in the month-to-month changes in beach areas, (as well as for the remaining coverage classes). To examine the correlations between socioeconomic indicators and built-up areas in each CM, we employed the correlation analysis approach. This method made it possible to evaluate the relationships between different time series, such as the trend in urban expansion and the population of each CM. This evaluation was based on Pearson's correlation coefficient[65], an index that measures the degree of linear relationship between two variables. Using this approach, it was possible to quantify the link between urban sprawl and population growth over the years for each CM. In addition, we conducted a correlation analysis between income and built-up area and between income and population.

Further, the Mann Kendall Test[66] was used to analyze trends related to changes in beach areas in each LICEL. This test made it possible to examine the temporal trends of coastal areas, providing important information on the trend of accretion or erosion of beaches in each LICEL area.

## Data availability

The datasets used and/or analysed during the current study available from the corresponding author on reasonable request.

## References

1. Gibbard, S., Caldeira, K., Bala, G., Phillips, T. J. & Wickett, M. Climate effects of global land cover change. *Geophys. Res. Lett.* **32**, 2005GL024550 (2005).
2. Perugini, L. et al. Biophysical effects on temperature and precipitation due to land cover change. *Environ. Res. Lett.* **12**, 053002 (2017).
3. Borrelli, P. et al. Land use and climate change impacts on global soil erosion by water (2015–2070). *Proc. Natl. Acad. Sci.* **117**, 21994–22001 (2020).
4. Froese, R. & Schilling, J. The nexus of climate change, land use, and conflicts. *Curr. Clim. Change Rep.* **5**, 24–35 (2019).
5. Bai, X., Jia, X., Jia, Y. & Hu, W. Modeling long-term soil water dynamics in response to land-use change in a semi-arid area. *J. Hydrol.* **585**, 124824 (2020).
6. Briassoulis, H. Factors influencing land-use and land-cover change. *Land. Cover Land Use Glob. Change Encycl. Life Support Syst. EOLSS* **1**, 126–146 (2009).
7. Harley, C. D. et al. The impacts of climate change in coastal marine systems. *Ecol. Lett.* **9**, 228–241 (2006).
8. Toimil, A., Losada, I. J., Nicholls, R. J., Dalrymple, R. A. & Stive, M. J. F. addressing the challenges of climate change risks and adaptation in coastal areas: A review. *Coast Eng.* **156**, 103611 (2020).
9. Toimil, A. et al. Climate change-driven coastal erosion modelling in temperate sandy beaches: Methods and uncertainty treatment. *Earth-Sci. Rev.* **202**, 103110 (2020).

10. Crain, C. M., Halpern, B. S., Beck, M. W. & Kappel, C. V. Understanding and managing human threats to the coastal marine environment. *Ann. N. Y. Acad. Sci.* **1162**, 39–62 (2009).
11. Spalding, M. D. et al. The role of ecosystems in coastal protection: adapting to climate change and coastal hazards. *Ocean. Coast Manag.* **90**, 50–57 (2014).
12. Desmet, K. et al. Evaluating the Economic Cost of Coastal Flooding. (2018).
13. Kummu, M. et al. Over the hills and further away from coast: Global geospatial patterns of human and environment over the 20th–21st centuries. *Environ. Res. Lett.* **11**, 034010 (2016).
14. Feng, Y. et al. Doubling of annual forest carbon loss over the tropics during the early twenty-first century. *Nat. Sustain.* **5**, 444–451 (2022).
15. Shilland, R. et al. A question of standards: adapting carbon and other PES markets to work for community seagrass conservation. *Mar. Policy* **129**, 104574 (2021).
16. García-Nieto, A. P. et al. Impacts of urbanization around Mediterranean cities: Changes in ecosystem service supply. *Ecol. Indic.* **91**, 589–606 (2018).
17. Salvati, L., Smiraglia, D., Bajocco, S. & Munafò, M. *Land Use Changes in Two Mediterranean Coastal Regions*8 (Do Urban Areas Matter?, 2014).
18. Kim, D., Sexton, J. O. & Townshend, J. R. Accelerated deforestation in the humid tropics from the 1990s to the 2000s. *Geophys. Res. Lett.* **42**, 3495–3501 (2015).
19. Winkler, K., Fuchs, R., Rounsevell, M. & Herold, M. Global land use changes are four times greater than previously estimated. *Nat. Commun.* **12**, 2501 (2021).
20. Findell, K. L. et al. The impact of anthropogenic land use and land cover change on regional climate extremes. *Nat. Commun.* **8**, 989 (2017).
21. Nath, A. et al. Assessing Coastal Land-Use and Land-Cover Change Dynamics using Geospatial techniques. *Sustainability* **15**, 7398 (2023).
22. Ngondo, J. et al. Land-Use and Land-Cover (LULC) Change Detection and the Implications for Coastal Water Resource Management in the Wami–Ruvu Basin, Tanzania. *Sustainability* **13**, 4092 (2021).
23. Foody, G. M. Status of land cover classification accuracy assessment. *Remote Sens. Environ.* **80**, 185–201 (2002).
24. Phiri, D. & Morgenroth, J. Developments in Landsat land cover classification methods: A review. *Remote Sens.* **9**, 967 (2017).
25. Grimes, M., Carrivick, J. L., Smith, M. W. & Comber, A. J. Land cover changes across Greenland dominated by a doubling of vegetation in three decades. *Sci. Rep.* **14**, 3120 (2024).
26. Thanh Noi, P. & Kappas, M. Comparison of random forest, k-nearest neighbor, and support vector machine classifiers for land cover classification using Sentinel-2 imagery. *Sensors* **18**, 18 (2018).
27. Zhou, H. & Liu, Y. Accurate integration of multi-view range images using k-means clustering. *Pattern Recognit.* **41**, 152–175 (2008).
28. Hussein, K., Alkaabi, K., Ghebreyesus, D., Liaqat, M. U. & Sharif, H. O. Land use/land cover change along the Eastern Coast of the UAE and its impact on flooding risk. *Geomat. Nat. Hazards Risk* **11**, 112–130 (2020).
29. Liu, P. et al. RS and LULC and UHI Change Simulation and Assessment. *J. Sens.* 1–17 (2020). (2020).
30. Wang, M., She, A., Chang, H., Cheng, F. & Yang, H. A deep inverse convolutional neural network-based semantic classification method for land cover remote sensing images. *Sci. Rep.* **14**, 7313 (2024).
31. Carranza-García, M., García-Gutiérrez, J. & Riquelme, J. C. A framework for evaluating land use and land cover classification using convolutional neural networks. *Remote Sens.* **11**, 274 (2019).
32. Chachondhia, P., Shakya, A. & Kumar, G. Performance evaluation of machine learning algorithms using optical and microwave data for LULC classification. *Remote Sens. Appl. Soc. Environ.* **23**, 100599 (2021).
33. Mansour, S., Ghoneim, E., El-Kersh, A., Said, S. & Abdelnaby, S. Spatiotemporal Monitoring of Urban Sprawl in a Coastal City using GIS-Based Markov Chain and Artificial neural network (ANN). *Remote Sens.* **15**, 601 (2023).
34. Shetty, S. Analysis of Machine Learning Classifiers for LULC Classification on Google Earth Engine.
35. Tassi, A. & Vizzari, M. Object-oriented LULC classification in Google earth engine combining SNIC, GLCM, and machine learning algorithms. *Remote Sens.* **12**, 3776 (2020).
36. Abdullah, A. Y. M. et al. Spatio-temporal patterns of land use/land cover change in the heterogeneous coastal region of Bangladesh between 1990 and 2017. *Remote Sens.* **11**, 790 (2019).
37. Feng, Q. et al. Integrating multitemporal sentinel-1/2 data for coastal land cover classification using a multibranch convolutional neural network: a case of the yellow river Delta. *Remote Sens.* **11**, 1006 (2019).
38. Clemente, M. F., D'Ambrosio, V. & Focareta, M. The proposal of the Coast-RiskBySea: COASTal zones RISK assessment for built environment bY extreme SEA level, based on the new Copernicus Coastal Zones data. *Int. J. Disaster Risk Reduct.* **75**, 102947 (2022).
39. Liu, X. et al. High-spatiotemporal-resolution mapping of global urban change from 1985 to 2015. *Nat. Sustain.* **3**, 564–570 (2020).
40. Truong, V. T. et al. JAXA's new high-resolution land use land cover map for Vietnam using a time-feature convolutional neural network. *Sci. Rep.***14**, 3926 (2024).
41. Buscombe, D. et al. A 1.2 billion Pixel Human-labeled dataset for Data-Driven classification of Coastal environments. *Sci. Data* **10**, 46 (2023).
42. Manno, G. et al. An Approach for the validation of a Coastal Erosion Vulnerability Index: An application in Sicily. *J. Mar. Sci. Eng.* **11**, 23 (2022).
43. van Vliet, J., Bregt, A. K. & Hagen-Zanker, A. Revisiting Kappa to account for change in the accuracy assessment of land-use change models. *Ecol. Model.* **222**, 1367–1375 (2011).
44. Iuppa, C., Cavallaro, L., Vicinanza, D. & Foti, E. Investigation of suitable sites for wave energy converters around Sicily (Italy). *Ocean. Sci.* **11**, 543–557 (2015).
45. Menna, M. et al. New insights of the Sicily Channel and southern Tyrrhenian Sea variability. *Water* **11**, 1355 (2019).
46. Monteforte, M., Re, C. L. & Ferreri, G. Wave energy assessment in Sicily (Italy). *Renew. Energy* **78**, 276–287 (2015).
47. Lo Re, C., Manno, G., Ciraolo, G. & Besio, G. Wave energy assessment around the Aegadian Islands (Sicily). *Energies* **12**, 333 (2019).
48. Romano, B., Zullo, F., Fiorini, L. & Marucci, A. Illegal building in Italy: Too complex a problem for national land policy? *Cities* **112**, 103159 (2021).
49. Zanfi, F. The Città Abusiva in Contemporary Southern Italy: Illegal building and prospects for change. *Urban Stud.* **50**, 3428–3445 (2013).
50. Angeli, F. The injured coast: The degradation of the Italian coastal landscape between unauthorized development, eco-mafia and regulations. (2019).
51. Cirelli, C., Mercatanti, L. & Porto, C. M. Sustainable development of Sicily east coast area. (2003).
52. Scepan, J. Thematic validation of high-resolution global land-cover data sets. *Photogramm Eng. Remote Sens.* **65**, 1051–1060 (1999).
53. Wang, Y. et al. A review of regional and global scale land Use/Land cover (LULC) mapping products generated from satellite remote sensing. *ISPRS J. Photogramm. Remote Sens.* **206**, 311–334 (2023).
54. Venter, Z. S., Barton, D. N., Chakraborty, T., Simensen, T. & Singh, G. Global 10 m land Use Land Cover datasets: a comparison of Dynamic World, World Cover and Esri Land Cover. *Remote Sens.* **14**, 4101 (2022).

55. Eea, F. Pkz048-99-v0 Massimo Zotti Claudio La Mantia.
56. Witjes, M. et al. A spatiotemporal ensemble machine learning framework for generating land use/land cover time-series maps for Europe (2000–2019) based on LUCAS, CORINE and GLAD landsat. *PeerJ* **10**, e13573 (2022).
57. Zhang, Y., Zhao, D., Zhang, J., Xiong, R. & Gao, W. Interpolation-dependent image downsampling. *IEEE Trans. Image Process.* **20**, 3291–3296 (2011).
58. Hirahara, D., Takaya, E., Kadowaki, M., Kobayashi, Y. & Ueda, T. Effect of the pixel interpolation method for downsampling medical images on deep learning accuracy. *J. Comput. Commun.* **9**, 150–156 (2021).
59. McGranahan, G., Balk, D. & Anderson, B. The rising tide: Assessing the risks of climate change and human settlements in low elevation coastal zones. *Environ. Urban* **19**, 17–37 (2007).
60. Ronneberger, O., Fischer, P. & Brox, T. U-Net: Convolutional Networks for Biomedical Image Segmentation. Preprint at http://arxiv.org/abs/1505.04597 (2015).
61. Buslaev, A. et al. Albumentations: fast and flexible image augmentations. *Information* **11**, 125 (2020).
62. Brownlee, A. E. I., Adair, J., Haraldsson, S. O. & Jabbo, J. Exploring the Accuracy – Energy Trade-off in Machine Learning. in *2021 IEEE/ACM International Workshop on Genetic Improvement (GI)* 11–18IEEE, Madrid, Spain, doi: https://doi.org/10.1109/GI52543.2021.00011 (2021).
63. Zheng, Q. H. et al. Accuracy comparison and driving factor analysis of LULC changes using multi-source time-series remote sensing data in a coastal area. *Ecol. Inf.* **66**, 101457 (2021).
64. Cohen, J. A coefficient of agreement for nominal scales. *Educ. Psychol. Meas.* **20**, 37–46 (1960).
65. Cohen, I. et al. Pearson correlation coefficient. *Noise Reduct. Speech Process* 1–4 (2009).
66. McLeod, A. I. Kendall rank correlation and Mann-Kendall trend test. *R Package Kendall* **602**, 1–10 (2005).

## Acknowledgements

## Author contributions

Pietro Scala dealt with: Data curation; Conceptualization; Formal analysis; Investigation; Methodology; Software; Validation; Visualization; Writing - original draft and Writing - review & editing. Alexandra Toimil dealt with: Conceptualization; Funding acquisition; Investigation; Methodology; Project administration; Resources; Supervision; Validation; Visualization and Writing - review & editing. Moisés Álvarez-Cuesta dealt with: Conceptualization; Investigation; Methodology; Supervision; Validation; Visualization and Writing - review & editing. Giorgio Manno dealt with: Data curation; Investigation; Supervision; Validation; Visualization; Roles/Writing - original draft and Writing - review & editing. Giuseppe Ciraolo dealt with: Investigation; Methodology; Supervision; Validation and Writing - review & editing. All authors contributed to the final version of the MS.

## Declarations

### Competing interests

The authors declare no competing interests.

### Additional information

**Publisher's note** Springer Nature remains neutral with regard to jurisdictional claims in published maps and institutional affiliations.